 SDHM, vol.2, no.4, pp.225-237, 2006

Numerical Evaluation of T-stress Solutions for Cracks in Plane Anisotropic Bodies

P.D. Shah[1], Ch. Song[2], C.L. Tan[1] and X. Wang[1]

Abstract: Numerical T-stress solutions in two dimensional anisotropic cracked bodies are very scarce in the literature. Schemes to evaluate this fracture parameter in anisotropy have been reported only fairly recently. Among them are those developed in conjunction with two different computational techniques, namely, the Boundary Element Method (BEM) and the Scaled Boundary Finite-Element Method (SBFEM). This paper provides a review of the respective schemes using these techniques and demonstrates their efficacy with three examples. These examples, which are of engineering importance, involve cracks lying in a homogeneous medium as well as at the interface between dissimilar media. The numerical T-stress solutions obtained by the two distinct numerical schemes are compared and they show excellent agreement with each other, further establishing the veracity of the two independent methodologies employed. They are also new additions to the very limited number of reference solutions in the literature, particularly for anisotropic elasticity.

keyword: T-stress, Anisotropic elasticity, Interface crack, Boundary element method, Scaled boundary finite-element method.

1 Introduction

Structural composites, single crystals, bicrystals and thermal barrier coatings are examples of advanced materials which are increasingly being used in engineering applications. The study of cracks in these components is important in order to assess their structural integrity. In conventional linear elastic fracture mechanics (LEFM), the severity of the stresses in the vicinity of the crack tip is characterized in terms of the leading singular terms in the Williams' (1957) eigenfunction series expansion, namely, the stress intensity factors. In two-dimensional homogenous materials, the stress intensity factors are primarily associated with the two modes of crack deformation, which are the opening mode K_I and the shear mode K_{II}. The definition of K_I and K_{II} are the same for both isotropic and anisotropic cracked homogeneous bodies. In the case of an interface crack between dissimilar materials, the near crack-tip stress singularity exhibits oscillatory behaviour [see, e.g., Williams (1959), Rice (1988), Suo (1990)] and the stress intensity factors are always coupled; they are usually represented as $\mathbf{K} = K_I + iK_{II}$, where $i = \sqrt{-1}$. Numerous schemes and computational methods have been developed over the years to obtain this fracture parameter for cracks in homogeneous isotropic and anisotropic bodies, as well as for interface cracks between dissimilar materials. They are now well established in the literature and thus the stress intensity factors will not be a focus of this paper.

The works of Larsson and Carlsson (1973), Rice (1974), Cotterell and Rice (1980), Leevers and Radon (1982), and Bilby *et al*. (1986), however, showed the importance of including the leading non-singular term of Williams' series expansion in explaining the stress constraint effects in the vicinity of the crack-tip. This leading non-singular term, commonly referred to as the elastic T-stress, is increasingly being recognized as an important second fracture parameter for fracture assessments [see, e.g., Betegon and Hancock (1991), Du and Hancock (1991), Ainsworth *et al*. (2000)]. Several analytical and numerical schemes for the evaluation of the T-stress in cracked, isotropic bodies have been developed over the years [see, e.g., Kfouri (1986), Sham (1991), Sladek *et al*. (1997), Wang (2002), Fett (2002), Tan and Wang (2003), Li *et al*. (2005)]. For non-isotropic bodies, however, similar studies on the determination of T-stress are relatively recent and scarce in number. Contributions in this regard include those by Ma *et al.* (1997), Yang and Yuan (2000), Kim and Paulino (2004), Song (2005) and Shah *et al.* (2006a). Those for bimaterial interface cracks between isotropic as well as anisotropic materials, suffer from similar scarcity. Among the few works on the evaluation of T-stress for interface cracks between dissimilar materials are the works of Sladek and Sladek (1997) and

[1] Carleton University, Ottawa, Canada
[2] University of New South Wales, Sydney, Australia

Fett and Rizzi (2004), for isotropy. Corresponding studies for such cracks between anisotropic bodies have been presented by Kim *et al.* (2001), Song (2005) and Shah *et al.* (2006b) all of whom have proposed independent schemes for the T-stress determination. However, only the last authors have presented numerical solutions for T-stress for cracks in homogeneous bodies and for interface cracks between dissimilar bodies in anisotropy. There is paucity of T-stress solutions for cracks in anisotropic bodies indeed, even if they are obtained primarily for the purpose of verification of new numerical schemes that are developed.

The Boundary Element Method (BEM) is now well established as a very efficient computational technique for LEFM analysis. Another more recently developed numerical technique which is also very well suited for fracture mechanics analysis is the Scaled Boundary Finite-Element Method (SBFEM) [Song (2005)]. It is a semi-analytical boundary element method based on finite elements; unlike in conventional BEM, no fundamental solutions are required in the formulation, and yet it has many of the characteristics of BEM modeling. As mentioned above, the present authors have recently developed distinctly different schemes for the determination of T-stresses for cracks in elastic, homogeneous anisotropic solids in conjunction with the BEM [Shah *et al*. (2006a, 2006b)] and with the SBFEM [Song (2005)]. These two numerical techniques can thus provide independent checks of T-stress solutions for new reference problems, to further demonstrate the veracity of the techniques for extracting this fracture parameter in numerical LEFM stress analysis. This is the aim of the present paper.

In the next section, the steps and formulation for the determination of T-stress for cracks in anisotropic elasticity using the BEM will first be reviewed and discussed. This will be followed by same when using the SBFEM. To demonstrate the veracity of these two relatively new approaches, three problems from engineering applications are analyzed and the numerical solutions obtained are compared. They could serve as additional reference results in the literature, in view of the paucity of these solutions in anisotropy.

2 Determination of T-stress using Boundary Element Method

The BEM for two-dimensional anisotropic elasticity is well established in the literature and it is also well recognized as an efficient numerical tool for obtaining stress intensity factors in linear elastic fracture mechanics analysis [see, e.g., Tan and Gao (1990, 1992)]. Hence their formulations will not be discussed here. The schemes for the determination of T-stress for cracks in plane, anisotropic bodies using the BEM have recently been proposed by Shah *et al.* (2006a, 2006b). The key steps applicable to an interface crack between dissimilar anisotropic bodies will be briefly reviewed here; it is equally applicable to a crack in a homogenous body. The method is based on the mutual or M-integral and utilizes the field values at points remote from the crack tip, thereby yielding more reliable and accurate results. With reference to Fig. 1, the field points are located along the contour Γ_o of the path-independent J-integral given as

$$J = \int_{\Gamma_0} (W n_1 - t_i u_{i,1})\, d\Gamma \tag{1}$$

where W is the strain energy density; u_i and t_i are the displacement and tractions respectively; and $n_j$is the unit outward normal vector of the contour (i, j = 1,2).

Defining the J-integral for two independent equilibrium states A and *aux*, the M-integral, is expressed in terms of $J-$integral as follows,

$$M = J^{(A+aux)} - J^{(A)} - J^{(aux)} \tag{2}$$

where

$$J^{(A)} = \int_{\Gamma_0} \left[\frac{1}{2} \left(\sigma_{ij}^A \varepsilon_{ij}^A n_1 \right) - \sigma_{ij}^A n_j u_{i,1}^A \right] d\Gamma \tag{3a}$$

$$J^{(aux)} = \int_{\Gamma_0} \left[\frac{1}{2} \left(\sigma_{ij}^{aux} \varepsilon_{ij}^{aux} n_1 \right) - \sigma_{ij}^{aux} n_j u_{i,1}^{aux} \right] d\Gamma \tag{3b}$$

Thus,

$$M = \int_{\Gamma_0} \left(\sigma_{ij}^A \varepsilon_{ij}^{aux} n_1 - \sigma_{ij}^A n_j u_{i,1}^{aux} - \sigma_{ij}^{aux} n_j u_{i,1}^A \right) d\Gamma \tag{4}$$

In Eqs. (2)-(4), the superscripts A denote the field solutions under study, and *aux* denote the auxiliary set of solutions. The auxiliary solutions are chosen here to correspond to those due to a point (line) force f applied at the interface crack-tip along the crack plane of a semi-infinite crack as shown in Fig. 1. For a bimaterial interface crack, the available solution for a composite wedge

subjected to a point force at the apex [Chung and Ting (1995)] is utilized to obtain the auxiliary fields given below by setting the wedge angle equal to 2π. The displacement gradients and the stresses in the global $X_1 - X_2$ Cartesian coordinate system may be written as

$$u_{i,j}^{(w)aux} = \frac{1}{\pi r}\left\{-h_i n_j(\theta) - (\mathbf{N}_1(\theta)\,\mathbf{h})_i m_j(\theta)\right\} \tag{5}$$

$$\sigma_{1j}^{(w)aux} = \frac{1}{\pi r}\left[\mathbf{N}_3(\theta)\,\mathbf{h}\right]_j m_2(\theta) \tag{6a}$$

$$\sigma_{2j}^{(w)aux} = -\frac{1}{\pi r}\left[\mathbf{N}_3(\theta)\,\mathbf{h}\right]_j m_1(\theta) \tag{6b}$$

where w corresponds to the $w-$th material (for bimaterial interface, w = 1,2), and

$$\begin{aligned} &n_1(\theta) = \cos\theta; \quad n_2(\theta) = \sin\theta; \\ &m_1(\theta) = -\sin\theta; \;\; m_2(\theta) = \cos\theta \end{aligned} \tag{7}$$

Also, in Eqs.(5)-(6), $\mathbf{N}_i$ are the elements of the fundamental elasticity matrix $\mathbf{N}$ [see, e.g., Ingebrigtsen and Tonning (1969)] given as

$$\mathbf{N}_1(\omega) = -\mathbf{T}^{-1}(\omega)\mathbf{R}^T(\omega) \tag{8a}$$

$$\mathbf{N}_2(\omega) = \mathbf{T}^{-1}(\omega) \tag{8b}$$

$$\mathbf{N}_3(\omega) = \mathbf{R}(\omega)\mathbf{T}^{-1}(\omega)\mathbf{R}^T(\omega) - \mathbf{Q}(\omega) \tag{8c}$$

where ω is the angle of inclination of the interface crack with respect to the x_1-axis (see Fig. 1), and

$$Q = \begin{bmatrix} C_{1111} & C_{1121} \\ C_{1121} & C_{2121} \end{bmatrix} = \begin{bmatrix} \mathbf{C}_{11} & \mathbf{C}_{16} \\ \mathbf{C}_{16} & \mathbf{C}_{66} \end{bmatrix} \tag{9a}$$

$$R = \begin{bmatrix} C_{1112} & C_{1122} \\ C_{2112} & C_{2122} \end{bmatrix} = \begin{bmatrix} \mathbf{C}_{16} & \mathbf{C}_{12} \\ \mathbf{C}_{66} & \mathbf{C}_{26} \end{bmatrix} \tag{9b}$$

$$T = \begin{bmatrix} C_{1212} & C_{1222} \\ C_{1222} & C_{2222} \end{bmatrix} = \begin{bmatrix} \mathbf{C}_{66} & \mathbf{C}_{26} \\ \mathbf{C}_{26} & \mathbf{C}_{22} \end{bmatrix} \tag{9c}$$

$\mathbf{C}$ in Eq.(9) being the reduced stiffness matrix for the material.

The elasticity matrices, $\mathbf{Q}(\omega)$, $\mathbf{R}(\omega)$, $\mathbf{T}(\omega)$ are obtained from $\mathbf{Q}$, $\mathbf{R}$, $\mathbf{T}$ following the transformation law with the rotated local coordinates, as

$$\mathbf{Q}(\omega) = \mathbf{Q}\cos^2\theta + (\mathbf{R} + \mathbf{R}^T)\sin\theta\cos\theta + \mathbf{T}\sin^2\theta \tag{10a}$$

$$\mathbf{R}(\omega) = \mathbf{R}\cos^2\theta + (\mathbf{T} - \mathbf{Q})\sin\theta\cos\theta - \mathbf{R}^T\sin^2\theta \tag{10b}$$

$$\mathbf{T}(\omega) = \mathbf{T}\cos^2\theta - (\mathbf{R} + \mathbf{R}^T)\sin\theta\cos\theta + \mathbf{Q}\sin^2\theta \tag{10c}$$

Furthermore, the vector **h,** which remains invariant for both materials forming the interface, is given as

$$\mathbf{h} = \overline{L}^{-1}\mathbf{f} \tag{11}$$

where

$$\overline{L} = \frac{1}{\pi}\int_{\theta_0}^{\theta_n} -N_3(\omega)\,d\omega \tag{12}$$

and $\mathbf{f}$ is the point force vector applied at the wedge apex, *i.e.*

$$\mathbf{f} = \begin{Bmatrix} f_1 \\ f_2 \end{Bmatrix} \tag{13}$$

The M-integral expression in Eq. (4) inherits the property of path independence from J-integrals. Thus, considering an arbitrary contour radius ε when shrunk to zero, it becomes

$$M = \lim_{\varepsilon\to 0}\int_{\Gamma_\varepsilon} (\sigma_{ij}^A \varepsilon_{ij}^{aux} n_1 - \sigma_{ij}^A n_j u_{i,1}^{aux} - \sigma_{ij}^{aux} n_j u_{i,1}^A)\,d\Gamma \tag{14}$$

Since the M and J-integrals are bounded, there is no contribution from the singular terms in M-integral in Eq. (14). The asymptotic field in state A can be separated into singular and non-singular components designated with s and T, respectively as follows:

$$\sigma_{ij}^A = \sigma_{ij}^s + \sigma_{ij}^T \tag{15}$$

$$u_{ij}^A = u_{ij}^s + u_{ij}^T \tag{16}$$

Thus, the contour integral from θ = -π to +π leaves only the non-vanishing contribution from the T-stress, and the M-integral reduces to

$$M = \lim_{\varepsilon\to 0}\int_{\Gamma_\varepsilon} (\sigma_{ij}^T \varepsilon_{ij}^{aux}\delta_{1j} - \sigma_{ij}^T u_{i,1}^{aux} - \sigma_{ij}^{aux} u_{i,1}^T)\,n_j d\Gamma \tag{17}$$

where it can be shown that

$$\sigma_{ij}^T = \frac{a_{11}^{\prime(2)}}{a_{11}^{\prime(1)}} T\delta_{i1}\delta_{j1}, \text{ for } 0 \le \theta \le \pi(material - 1) \tag{18}$$

$$\sigma_{ij}^{T} = T\delta_{i1}\delta_{j1} \text{ for } -\pi \leq \theta \leq 0 (material-2) \tag{19}$$

T in Eqs.(18) and (19) being the T-stress along material-2.

Finally, Eq. (17) reduces to

$$M = Ta_{11}^{'(2)} f \tag{20}$$

or,

$$T = \frac{M}{a_{11}^{'(2)} f} \tag{21}$$

where $a_{11}^{'(2)}$ corresponds to the first element of the elastic compliance matrix for the material-2 in the local coordinates $X_i^{'}$. The T-stress values in material 1 and 2 are related as

$$T^{(1)} a_{11}^{'(1)} = T^{(2)} a_{11}^{'(2)} \tag{22}$$

In the present work, the values of the T-stress obtained are with reference to material-2.

Also, in the case of plane strain conditions, a_{11} should be replaced by b_{11} using [see, e.g., Tan and Gao (1992)]

$$b_{ij} = a_{ij} - a_{i3}a_{j3}/a_{33} \tag{23}$$

The M-integral should be evaluated in the local coordinate system $X_i^{'}$ using Eq. (4). In present work, the M-integral is first obtained in global coordinates and then transformed into local coordinates following the J-integral transformation by Kishimoto *et al.* (1980), as follows:

$$M_{(Local)} = M_{1(Global)} \cos\omega + M_{2(Global)} \sin\omega \tag{24}$$

where

$$M_{k(Global)} = \int_{\Gamma_0} (\sigma_{ij}^{A} \varepsilon_{ij}^{aux} n_k - \sigma_{ij}^{A} n_j u_{i,k}^{aux} - \sigma_{ij}^{aux} n_j u_{i,k}^{A}) \, d\Gamma \tag{25}$$

The scheme outlined above relies on the auxiliary field solutions based on Stroh's formalism [Chung and Ting, (1995)] and is applicable to both homogenous and interface crack materials. The authors [Shah *et al.* (2006a)] have also developed the M-integral formulation based on Lekhnitskii's formalism [Lekhnitskii (1968)] and it is applicable to homogenous cracked bodies.

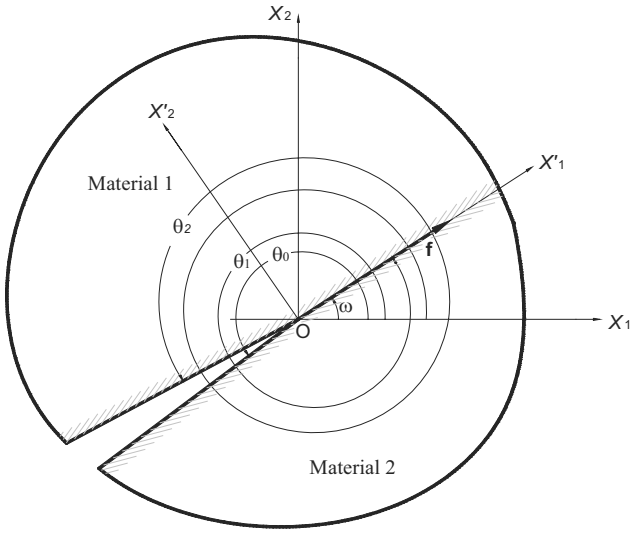

Figure 1 : A composite wedge comprising of two anisotropic materials and point force **f** applied at the apex.

3 Determination of T-stress using Scaled Boundary Finite-Element Method

The scaled boundary finite-element method was originally developed for the dynamic analysis of unbounded domains [Wolf and Song (1996)]. At the initial stage of the development, it is called the consistent infinitesimal finite-element cell method reflecting the technique used in the derivation. The term "scaled boundary finite-element method" was used for the first time in Song and Wolf (1997), where the scaled boundary transformation is introduced and the application is extended to bounded domains. An appealing feature of this method in LEFM is that the solution in the radial direction passing through the scaling centre is obtained analytically without any *a priori* assumptions. Therefore, the stress singularity occurring at the crack tip can be conveniently modeled by choosing the scaling centre there. Using this technique, Song and Wolf (2002) analyzed the orders of singularity and stress intensity factors for multi-material plates, while Lindemann and Becker (2002) studied the free-edge stresses around holes in laminates. Similarly, Song (2004a) has obtained dynamic stress intensity factors, and Müller *et al.* (2005) have obtained predictions of the directions of cracks emerging from notches at bimaterial junctions. This method has been further extended to include the power-logarithmic singularities, and to cal-

culate orders of singularity, T-stresses and higher order terms under mechanical loading in Song, (2005). Singular stress field under thermal loading has also been investigated in Song (2006).

The derivation of the scaled boundary finite-element method is detailed in Song and Wolf (1997, 2000). The evaluation of T-stresses is addressed in Song (2005). Only the main concepts are summarized in this paper.

As an example, a multi-material wedge made of four materials shown in Fig. 2a is considered. A scaling centre O is chosen at the multi-material corner. Only the boundary S is discretized. The geometry of a line element is interpolated using the shape functions $[N(\eta)]$ formulated in the local coordinate η and the nodal coordinates $\{x\}$and$\{y\}$. As explained later, the two faces OA and OB and the material interfaces passing through the scaling centre are defined by a constant η, and are not discretized. The domain is described by scaling the boundary with the dimensionless radial coordinate ξ pointing from the scaling centre O to a point on the boundary. With no loss of generality, the origin of the Cartesian co-ordinates $(\hat{x}, \hat{y})$ is placed at the scaling centre. $\xi = 0$ at O, and $\xi = 1$ on the boundary are chosen

$$\{x(\xi,\eta)\} = \xi[N(\eta)]\{x\}$$
$$\{y(\xi,\eta)\} = \xi[N(\eta)]\{y\} \tag{26}$$

ξ, η are called the scaled boundary coordinates.

The scaled boundary coordinates in two dimensions resemble the polar coordinates $\hat{r}$ and θ. The boundary S of the problem domain V in Figure 2a is transformed to a circle described by a constant radial coordinate $\xi = 1$ (Fig. 2b) in the scaled boundary coordinates. The domain V is thus specified by $0 \le \xi \le 1$. A straight line, such as the side faces OA and OB and material interface OF, passing through the scaling center O remains as a straight line and is described by a constant η. When the origin of a polar coordinate system coincides with the scaling centre as in Fig. 2b, the radial coordinate $\hat{r}$ is expressed in the scaled boundary co-ordinates as

$$\hat{r}(\xi,\eta) = \xi r(\eta) = \xi\sqrt{x^2(\eta)+y^2(\eta)} \tag{27}$$

where $r(\eta)$ is the radial coordinate on the boundary. The angle θ is represented in a discretized form by the element number and the local coordinate η

$$\theta(\eta) = \arctan\frac{y(\eta)}{x(\eta)} \tag{28}$$

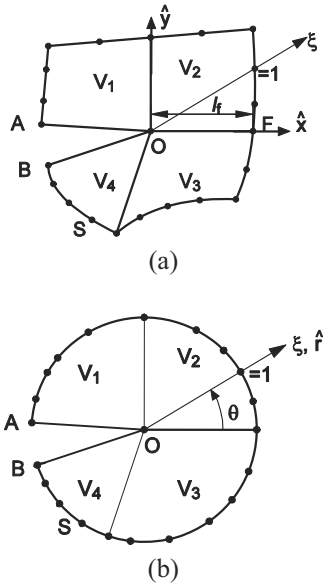

Figure 2 : Representation of multi-material wedge in scaled boundary coordinates: (a) scaling centre O, radial coordinate ξ and boundary discretization; (b) transformed domain.

As the whole boundary is visible from the scaling center, $\theta(\eta)$ is a single-valued function in its principal value $(-\pi < \theta \le \pi)$.

Along the radial lines passing through the scaling centre O and a node on the boundary (Fig. 2) the nodal displacement functions $\{u(\xi)\}$ are introduced. The displacements in the domain at a point (ξ,η) are interpolated from the nodal functions

$$\{u(\xi,\eta)\} = [N^u(\eta)]\{u(\xi)\} \tag{29}$$

where $[N^u(\eta)]$ denotes the shape functions for displacement interpolation. In this paper, isoparametric high-order elements with Gauss-Lobatto shape functions are used. After performing the scaled boundary transformation and applying the weighted residual technique in η direction, the scaled boundary finite-element equation in displacement is written as

$$[E^0]\xi^2\{u(\xi)\}_{,\xi\xi} + ([E^0] - [E^1] + [E^1]^T)\xi\{u(\xi)\}_{,\xi} - [E^2]\{u(\xi)\} = 0 \tag{30}$$

where $[E^0]$, $[E^1]$ and $[E^2]$ are coefficient matrices. Body forces, as discussed in Song (2006), are not considered in

this paper. The strains are expressed in the scaled boundary coordinates as

$$\{\varepsilon(\xi,\eta)\} = [B^1(\eta)]\{u(\xi)\}_{,\xi} + \xi^{-1}[B^2(\eta)]\{u(\xi)\} \tag{31}$$

where $[B^1(\eta)]$ and $[B^2(\eta)]$ depend on the geometry of the boundary only.

The solution of Eq. (30) for the displacement functions is expressed as (Song, 2004)

$$\{u(\xi)\} = \sum_{i=1}^{N} [\Psi_{ui}]\xi^{-[S_i]}\{c_i\} \tag{32}$$

Where $[S_i]$ is the ith block of the block-diagonal decomposition of a matrix constructed from $[E^0]$, $[E^1]$ and $[E^2]$. The real parts of the eigenvalues of $[S_i]$ are equal to zero or negative. The displacements are thus finite within the domain $(0 \le \xi \le 1)$. The term $[\Psi_{ui}]$ contains the Ritz vector and $\{c_i\}$ denotes the integration constants which are determined from the boundary conditions. The stresses are obtained by substituting the displacement solution, Eq. (32), into Eq. (31).

$$\{\sigma(\xi,\eta)\} = \sum_{i=1}^{N} [D][\Psi_{\sigma i}(\eta)]\xi^{-[S_i]-[I]}\{c_i\} \tag{33}$$

where $[D]$ is the elasticity matrix and $[\Psi_{\sigma i}(\eta)]$ denotes the stress modes. When the real parts of the eigenvalues in a diagonal block $[S_i]$ satisfy $-1 < Re(\lambda([S_i])) < 0$, the stresses in the corresponding term are singular. When multiple eigenvalues with parallel eigenvectors appear in a diagonal block $[S_i]$, power-logarithmic functions occur in the stress solutions. The extraction of the stress intensity factors is discussed in Song (2006).

The T-stress is evaluated by addressing the diagonal block satisfying $\lambda([S_i]) = -1$. The stresses in the corresponding term in Eq. (33) are expressed as (with a superscript T instead of the subscript i)

$$\{\sigma^T(\eta)\} = [\Psi^T_\sigma(\eta)]\{c^T\} \tag{34}$$

The stresses $\{\sigma^T(\eta)\}$ in the global coordinates are computed element-by-element at discrete Gauss integration points together with the angle $\theta(\eta)$. The stresses $\{\sigma^T\}_{(\text{Global})}$ at a specified angle θ are obtained by interpolation. The stresses $\{\sigma^T\}_{(\text{Local})}$ in the local coordinates (X_i in Figure 1) where the T-stress is defined can be evaluated by transformation from $\{\sigma^T\}_{(\text{Global})}$. The T-stress is the x-component of $\{\sigma^T\}_{(\text{Local})}$. Note that the singular stress field is not computed when evaluating the T-stress.

4 Results and Discussion

The methodologies presented above to extract T-stress in cracked anisotropic elastic bodies using the two independent numerical tools, namely BEM and SBFEM, have been applied to some problems of practical engineering importance. The results obtained using these two approaches are compared to test their veracity. In the first example, an inclined fault crack lying along the interface between dissimilar anisotropic sedimentary rocks is analyzed. The second example is the problem of a crack emanating from a fastener hole in a large anisotropic plate. Finally, a single edge crack in a bicrystal YCBO junction used in electronic applications is considered.

4.1 Example 1

Table 1 : Elastic mechanical properties of sandstone and dolomite reservoir rock.

Elastic Constants	Sandstone (Material 1)	Dolomite (Material 2)
E_{11}	16.59 GPa	61.46 GPa
E_{22}	17.95 GPa	47.61 GPa
E_{33}	20.39 GPa	55.6 GPa
G_{12}	7.67 GPa	20 GPa
G_{23}	8.23 GPa	23.3 GPa
G_{31}	7.53 GPa	24.38 GPa
v_{12}	0.167	0.153
v_{13}	0.142	0.173
v_{23}	0.156	0.171
$\eta_{12,1}$	0.025	– 0.142
$\eta_{12,2}$	–0.137	0.033
$\eta_{12,3}$	–0.022	–0.015
$\mu_{31,23}$	–0.087	–0.064

Fault cracks lying between different layers of rock are of great interest in civil engineering and geotechnical fields. For illustration here, a fault crack lying along the interface between sandstone reservoir rock (Material 1) and dolomite reservoir rock (Material 2) in a large domain is investigated. These rocks both demonstrate general anisotropic mechanical behaviour, their elastic properties

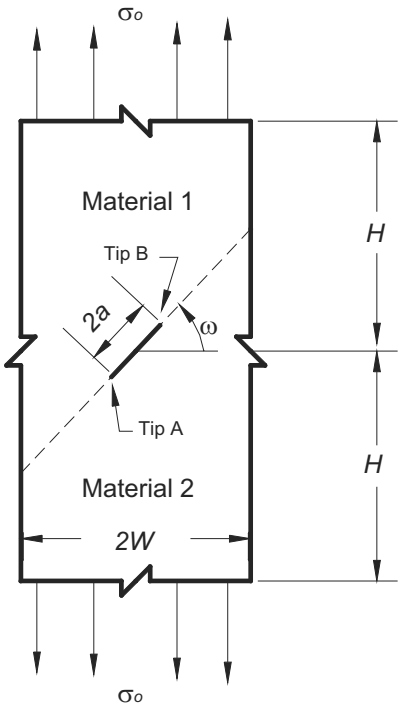

Figure 3 : A large plate with a central crack located along the interface between dissimilar anisotropic rocks.

Table 2 : Normalised T-stress for an interface crack in a large rectangular domain comprising sandstone and dolomite.

ω °	T/σ_o					
	Tip A			Tip B		
	BEM	SBFEM	% Diff	BEM	SBFEM	% Diff
0	-1.7318	-1.7317	0.01	-1.7309	-1.7308	0.01
15	-1.5507	-1.5450	0.37	-1.5503	-1.5534	-0.20
30	-0.8324	-0.8273	0.61	-0.8248	-0.8303	-0.67
45	0.0180	0.0175	2.78	0.0333	0.0326	2.10
60	0.7920	0.7879	0.52	0.8112	0.8097	0.18

in the principal axes directions are as given in Table 1 [Rasolofosaon and Zinszner (2002)].

For the purpose of analysis, the numerical solution domain is taken to be rectangular, as shown in Fig. 3, with $H/W = 2$, and the relative size of the interface crack, $a/W = 0.1$; the bimaterial continuum is subject to remote uniform tension σ_o. Plane strain conditions are assumed and the material principal axes for both rocks

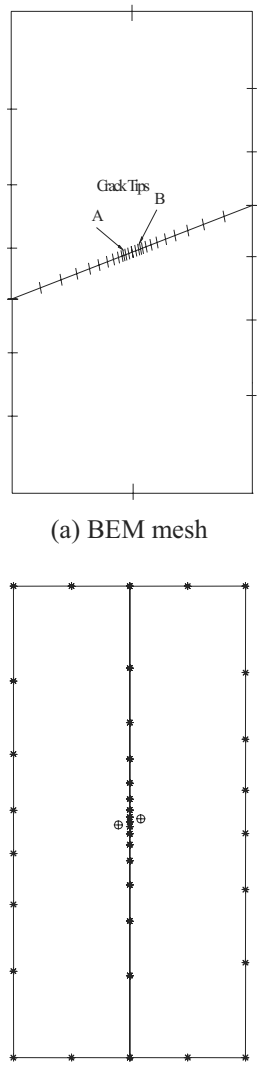

(a) BEM mesh

(b) SBFEM mesh

Figure 4 : The BEM and SBFEM meshes: Example 1. ω=15^o

are arbitrarily chosen to coincide with the global Cartesian axes. The angle of inclination of the interface between the rocks, ω, where the crack lies, is varied from 0^o to 60^o in 15^oincrements. Fig. 4 shows the BEM and the corresponding SBFEM mesh used. The BEM mesh contains two sub-regions for the problem and traction-singular quarter-point elements are used at the crack-tips. In the SBFEM mesh, the plate is divided into two sub-domains by a vertical line at the middle of the plate. Each sub-domain contains one crack tip. The scaling centres, indicated by the marker '$\oplus$', are located at the crack tips. The boundary of a sub-domain is divided into elements.

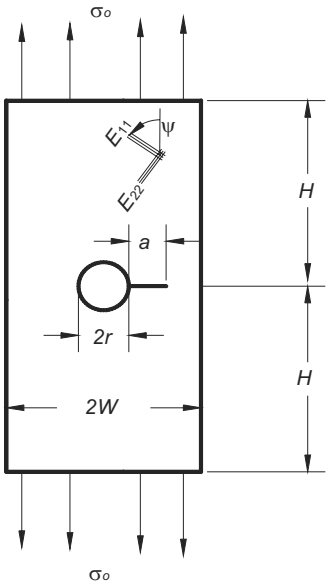

Figure 5 : Crack emanating from a circular hole in a rectangular plate.

The ends of an element is marked by '∗'. The crack faces passing through the scaling centres are not discretized and thus are not shown on the mesh. High-order isoparametric elements with Gauss-Lobatto shape functions are employed. *P*-refinement of the mesh is carried out until the difference between the T-stress from two successive refinements is less than 1%. The numerical results obtained from the two computational techniques are listed in Table 2. It can be seen that the normalised T-stress becomes increasingly less negative in magnitude at both the interface crack tips as the angle of inclination, ω, is increased and becomes positive when $\omega \geq 45^o$, signifying increasing stress constraint at the crack-tips. It is also evident that the agreement of the numerical results obtained using both numerical methods is excellent indeed; the discrepancies are, in general, less than one percent.

4.2 Example 2

The second example considered is the problem of a crack emanating from a circular hole in a rectangular composite material plate. This has important applications in, for example, the aerospace industry. The composite material considered is graphite-epoxy and its elastic engineering constants along the material principal axes directions are as follows [Tan and Gao (1992)]:

E_{11}= 144.8 GPa; E_{22}=11.7 GPa; G_{12}= 9.66 GPa; v_{12}=0.21

Table 3 : Normalised T-stress for a crack emanating from a circular hole in a graphite/ epoxy plate.

ψ^o	a/r	T/σ_o (BEM)	T/σ_o (SBFEM)	% Diff
0	0.05	-0.3612	-0.3664	-1.44
	0.1	-0.2343	-0.2383	-1.71
	0.2	-0.1649	-0.1669	-1.21
	0.3	-0.1552	-0.1561	-0.58
	0.4	-0.1607	-0.1607	0.00
	0.5	-0.1706	-0.1699	0.41
30	0.05	-0.3054	-0.3067	-0.43
	0.1	-0.2528	-0.2563	-1.38
	0.2	-0.1207	-0.1244	-3.07
	0.3	-0.0977	-0.0977	0.00
	0.4	-0.1248	-0.1222	2.08
	0.5	-0.1599	-0.1558	2.56
60	0.05	-0.5631	-0.5585	0.82
	0.1	-0.4950	-0.4893	1.15
	0.2	-0.3816	-0.3782	0.89
	0.3	-0.2915	-0.2904	0.38
	0.4	-0.2229	-0.2229	0.00
	0.5	-0.1772	-0.1770	0.11
90	0.05	-4.0512	-4.0187	0.80
	0.1	-3.6562	-3.6282	0.77
	0.2	-3.0616	-3.0416	0.65
	0.3	-2.6502	-2.6375	0.48
	0.4	-2.3684	-2.3580	0.44
	0.5	-2.1744	-2.1660	0.39

The geometry analysed is shown in Fig. 5, with H/W =2, r/W =0.1. Several crack sizes are considered, with crack length to the hole radius ratio, a/r, ranging from 0.05 to 0.5. The crack size is intentionally taken to be relatively small to study the effects of the stress concentration introduced by the circular hole on the obtained T-stress values. The angle of orientation of principal material axes with the global Cartesian axes, ψ, is also varied from 0^o to $90^o$to study its effects on this fracture parameter. It should be noted that E_{11} being the higher modulus, is oriented along the load direction x_2. The plate is subjected to remote uniform tension σ_o and plane stress conditions are assumed. Fig. 6 shows the typical BEM and the SBFEM meshes employed for the stress analysis of this problem for the same geometry. The results for the variation of the normalised T-stress with the "material angle"

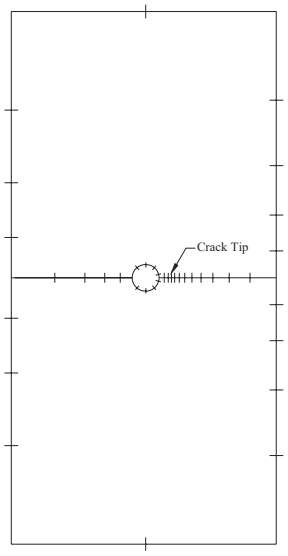

(a) BEM mesh

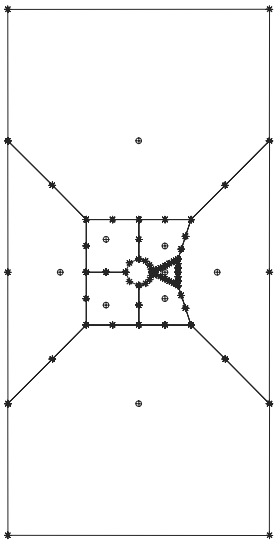

(b) SBFEM mesh

Figure 6 : BEM and SBFEM meshes: Example 2 (a/r=1).

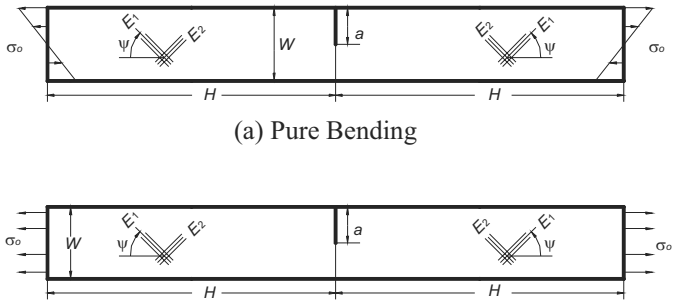

(a) Pure Bending

(b) Remote Tension

Figure 7 : A bicrystal with an edge crack.

constraints at the crack-tip. As expected, their magnitudes become significantly larger when $\psi = 90^o$ when compared to the case when $\psi = 0^o$, due to the higher modulus in the direction of the load application in latter case.

4.3 Example 3

Bicrystal interface materials are extensively being used in electronic applications for their excellent superconductive properties. A flaw along the bicrystal interface junction is another good example of an interface crack between dissimilar anisotropic materials. A bicrystal junction between YCBO ($YBa_2Cu_3O_7$) crystals is studied here. Such bicrystals are used in, e.g. Josephson junctions used in super-sensitive magnetometers (SQUIDs).

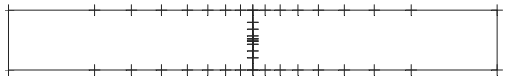

(a) BEM mesh

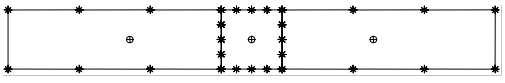

(b) SBFEM mesh

Figure 8 : BEM and SBFEM meshes: Example 3.

ψ and relative crack size, a/r, are presented in Table 3. Again, it can be seen that the results from SBFEM agree very well with the corresponding values from BEM. Of significance to note is that the computed values of the normalised T-stress are all negative, signifying low stress

For the purpose of illustration of the numerical analysis here, a single edge crack is introduced along the bicrystal interface or junction as shown in Fig. 7. The range of values of the geometric parameters analysed are: H/W = 4, a/W= 0.1, 0.2, 0.3, 0.4 and 0.5. Plane stress conditions are assumed and the specimen is subjected to pure

Table 4 : Normalised T-stress, T/σ_o, for an interface crack along a YCBO bicrystal junction for pure bending.

ω^o	a/W	T/σ_o		
		Pure Bending		
		BEM	SBFEM	%Diff
0	0.1	-0.3327	-0.3331	-0.12
	0.2	-0.2099	-0.2100	-0.05
	0.3	-0.0698	-0.0698	0.00
	0.4	0.1062	0.1065	-0.28
	0.5	0.3494	0.3504	-0.29
15	0.1	-0.3012	-0.3015	-0.10
	0.2	-0.1750	-0.1751	-0.06
	0.3	-0.0243	-0.0243	0.00
	0.4	0.1716	0.1720	-0.23
	0.5	0.4502	0.4513	-0.24
30	0.1	-0.2859	-0.2862	-0.10
	0.2	-0.1533	-0.1534	-0.07
	0.3	0.0103	0.0103	0.00
	0.4	0.2277	0.2282	-0.22
	0.5	0.5426	0.5439	-0.24
45	0.1	-0.2927	-0.2930	-0.10
	0.2	-0.1515	-0.1516	-0.07
	0.3	0.0248	0.0249	-0.40
	0.4	0.2610	0.2616	-0.23
	0.5	0.6052	0.6067	-0.25
60	0.1	-0.3241	-0.3244	-0.09
	0.2	-0.1739	-0.1740	-0.06
	0.3	0.0116	0.0117	-0.69
	0.4	0.2582	0.2588	-0.23
	0.5	0.6154	0.6169	-0.24
75	0.1	-0.3745	-0.3748	-0.08
	0.2	-0.2177	-0.2178	-0.05
	0.3	-0.0303	-0.0302	0.33
	0.4	0.2134	0.2139	-0.23
	0.5	0.5599	0.5613	-0.25
90	0.1	-0.4281	-0.4285	-0.09
	0.2	-0.2700	-0.2701	-0.04
	0.3	-0.0898	-0.0898	0.00
	0.4	0.1367	0.1371	-0.26
	0.5	0.4496	0.4508	-0.27

bending and pure tension. The following material properties are assumed for both crystals [elastic properties in [100]-crystal planes at 300K, Ramakrishnan and Krishnamurthy (1991)]:

E_{11}= 118.33 GPa; E_{22}= 91.99 GPa; G_{12}= 42.31 GPa; and v_{12}= 0.268.

with the principal axes oriented at $\pm\psi$ with respect to the Cartesian axes, as shown in Fig. 7. The values of ψ investigated are 0^o, 15^o, 30^o, 45^o, 60^o, $75^o$and 90^o

Fig. 8 shows the typical meshes employed for the stress analysis. The computed results are listed in Tables 4 and 5 where excellent agreement between the corresponding sets of results from the two computational techniques is again observed. It is interesting to note that the T-stress for the uniform remote tension load case all showed negative values; this is not true, however, for the pure bending case where the crack-tip stress constraint becomes increasing enhanced as the interface crack gets progressively larger. From the numerical results, the orientation of the material principal axes evidently also has an effect on the T-stress, although not as significantly as the change in the crack size.

5 Conclusions

The T-stress is increasingly being recognized as an important second characterizing parameter for fracture assessments. For plane anisotropic elasticity, numerical solutions of this parameter, even for reference purposes, are very scarce indeed. Different schemes to determine this parameter for plane anisotropic elasticity have recently been independently developed in conjunction with the Boundary Element Method (BEM) and Scaled Boundary-Finite Element Method (SBFEM). They have been reviewed in this paper and three practical examples have been analysed by these two independent approaches. Excellent agreement of the numerical results has been obtained which demonstrates their veracity. These problems and solutions could serve as reference cases for future studies in this area by alternative techniques.

References

Ainsworth, R.A.; Sattari, I.F.; Sherry, A.H.; Hooton, D.G.; Hadley, I. (2000): Methods for including constraint effects within SINTAP procedures. *Engineering Fracture Mechanics*, Vol. 67, pp. 563-571.

Betegon, C.; Hancock, J.W. (1991): Two-parameter characterization of elastic-plastic crack tip fields. *ASME Journal of Applied Mechanics*, Vol. 58, pp. 104-110.

Table 5 : Normalised T-stress, T/σ_o, for an interface crack along a YCBO bicrystal junction for remote tension.

ω^o	a/W	T/σ_0		
		Remote Tension		
		BEM	SBFEM	% Diff
0	0.1	-0.4852	-0.4851	0.02
	0.2	-0.5194	-0.5193	0.02
	0.3	-0.5382	-0.5381	0.02
	0.4	-0.5100	-0.5098	0.04
	0.5	-0.3725	-0.3719	0.16
15	0.1	-0.4569	-0.4567	0.04
	0.2	-0.4840	-0.4838	0.04
	0.3	-0.4872	-0.4871	0.02
	0.4	-0.4277	-0.4275	0.05
	0.5	-0.2271	-0.2263	0.35
30	0.1	-0.4473	-0.4470	0.07
	0.2	-0.4697	-0.4694	0.06
	0.3	-0.4611	-0.4609	0.04
	0.4	-0.3757	-0.3753	0.11
	0.5	-0.1198	-0.1188	0.83
45	0.1	-0.4634	-0.4632	0.04
	0.2	-0.4851	-0.4847	0.08
	0.3	-0.4713	-0.4711	0.04
	0.4	-0.3714	-0.3709	0.13
	0.5	-0.0813	-0.0801	1.48
60	0.1	-0.5073	-0.5070	0.06
	0.2	-0.5328	-0.5324	0.08
	0.3	-0.5230	-0.5228	0.04
	0.4	-0.4261	-0.4256	0.12
	0.5	-0.1358	-0.1347	0.81
75	0.1	-0.5684	-0.5680	0.07
	0.2	-0.6020	-0.6016	0.07
	0.3	-0.6060	-0.6057	0.05
	0.4	-0.5320	-0.5316	0.08
	0.5	-0.2823	-0.2814	0.32
90	0.1	-0.6243	-0.6239	0.06
	0.2	-0.6683	-0.6680	0.04
	0.3	-0.6923	-0.6922	0.01
	0.4	-0.6561	-0.6558	0.05
	0.5	-0.4790	-0.4783	0.15

Bilby, B.A.; Cardew, G.E.; Goldthorpe, M.R.; Howard, I.C. (1986): A finite element investigation of the effect of specimen geometry on the fields of stress and strain at the tips of stationary cracks. Size effects in Fracture. *London: Mechanical Engineering Publications Limited*, pp. 37-46.

Chung, M.Y.; Ting, T.C.T. (1995): Line force, charge, and dislocation in anisotropic piezoelectric composite wedges and spaces. *Journal of Applied Mechanics*, Vol. 62, pp. 423-428.

Cotterell, B.; Rice, J.R. (1980): Slightly curved or kinked cracks. *International Journal of Fracture*, Vol. 16, pp. 155-169.

Du, Z-Z, Hancock, J.W. (1991): The effect of non singular stresses on crack-tip constraint. *Journal of the Mechanics and Physics of Solids*, Vol. 39(4), pp. 555-567.

Fett, T. (2002): *T-stress solution and Stress Intensity Factors for 1-D cracks*. VDI Verlag, Germany.

Fett, T.; Rizzi, G. (2004): *Stress Intensity Factors and Constant Stress Terms for Interface Cracks*. Mitglied der Hermann von Helmholtz-Gemeinschaft Deutscher Forchungszentren (HGF).

Ingebrigtsen, K.A.; Tonning, A. (1969): Elastic surface waves in crystal. *Physics Review*, Vol. 184, pp. 942-951.

Kfouri, A.P. (1986): Some evaluations of the eastic T-term using Eshelby's method. *International Journal of Fracture*, Vol. 30, pp. 301-315.

Kim, J.H.; Moon, H.J.; Earmme, Y.Y. (2001): In-plane and antiplane T-stresses for an interface crack in anisotropic bimaterial. *Mechanics of Materials*, Vol. 33, pp. 21-32.

Kim, J.H.; Paulino, G.H. (2004): T-stress in orthotropic functionally graded materials: Lekhnitskii and Stroh formalisms. *International Journal of Fracture*, Vol. 126, pp. 345-384.

Kishimoto, K.; Aoki, S.; Sakata, M. (1980): On the path independent integral. *Engineering Fracture Mechanics*, Vol. 13, pp. 841-850.

Larsson, S.G.; Carlsson, A.J. (1973): Influence of non-singular stress terms and specimen geometry on small-scale yielding at crack tips in elastic-plastic materials. *Journal of the Mechanics and Physics of Solids*, Vol. 21, pp. 263-277.

Leevers, P.S.; Radon, J.C. (1982): Inherent stress biaxiality in various fracture specimen geometries. *International Journal of Fracture*, Vol. 19, pp. 311- 325.

Lekhnitskii, S.G. (1968): *Anisotropic Plates*. Gordon and Beach Science Publishers, New York, USA.

Li, J.; Tan, C.L.; Wang, X. (2005): Weight functions for T-stress for edge cracks in thick-walled cylinders. *Transactions of the ASME, Journal of Pressure Vessel Technology*, Vol. 127 (4), pp. 457-63.

Lindemann, J.; Becker, W. (2002): Free-edge stresses around holes in laminates by the boundary finite-element method. *Mechanics of Composite Materials*, Vol. 38, pp. 407-416.

Ma, H.; Zhao, L.G.; Chen, Y.H. (1997): Non-singular terms for multiple cracks in anisotropic elastic solids. *Theoretical and Applied Fracture Mechanics*, Vol. 27, pp. 129-134.

Müller, A.; Wenck, J.; Goswami, S.; Lindemann, J.; Hohe, J.; Becker, W. (2005): The boundary finite element method for predicting directions of cracks emerging from notches at bimaterial junctions. *Engineering Fracture Mechanics*. Vol. 72, pp. 373-386.

Ramakrishnan, C.; Krishnamurthy, N. (1991): The elastic constants of $YBa_2Cu_3O_{7t\delta}$. *Solid State Communications*, Vol. 79(4), pp. 363-369.

Rasolofosaon, P.N.J.; Zinszner, B.E. (2002): Comparison between permeability anisotropy and elasticity anisotropy of reservoir rocks. *Geophysics*, Vol. 67, pp. 230-240.

Rice, J.R. (1974): Limitations to the small scale yielding approximation for crack tip plasticity. *Journal of the Mechanics and Physics of Solids*, Vol. 22, pp. 17-26.

Rice, J.R. (1988): Elastic fracture mechanics concepts for interfacial cracks. *Journal of Applied Mechanics*, Vol. 54, pp. 98-103.

Shah, P.D.; Tan, C.L.; Wang, X. (2006a): T-stress solutions for two-dimensional crack problems in anisotropic elasticity using the Boundary Element Method. *Fatigue and Fracture of Engineering Materials and Structures*, Vol. 29(5), pp. 343-356.

Shah, P.D.; Tan, C.L.; Wang, X. (2006b): Evaluation of T-stress for an interface crack between dissimilar anisotropic materials using the Boundary Element Method. *CMES: Computer Modeling in Engineering & Sciences,* Vol. 13 (3), pp. 185-197.

Sham, T.L. (1991): The determination of the elastic T-term using higher order weight functions. *International Journal of Fracture*, Vol. 48, pp. 81-102.

Sladek, J.; Sladek, V. (1997): Evaluations of the T-stress for interface cracks by the boundary element method. *Engineering Fracture Mechanics*, Vol. 56(6), pp. 813-825.

Sladek, J.; Sladek, V.; Fedelinski, P. (1997): Contour integrals for mixed-mode crack analysis effect of nonsingular terms. *Theoretical and Applied Fracture Mechanics*, Vol. 27, pp. 115-127.

Song, Ch. (2004a): A super-element for crack analysis in the time domain. *International Journal for Numerical Methods in Engineering*, Vol. 61, pp. 1332–1357.

Song, Ch. (2004b): A matrix function solution for the scaled boundary finite-element equation in statics. *Computer Methods in Applied Mechanics and Engineering*, Vol. 193, pp. 2325-2356.

Song, Ch. (2005): Evaluation of power-logarithmic singularities, T-stresses and higher order terms of in-plane singular stress fields at cracks and multi-material corners. *Engineering Fracture Mechanics*, Vol. 72, pp. 1498-1530.

Song, Ch. (2006): Analysis of singular stress fields at multi-material corners under thermal loading. *International Journal for Numerical Methods in Engineering*, Vol. 65, pp. 620-652.

Song, Ch.; Wolf, J.P. (1997): The scaled boundary finite-element method - alias consistent infinitesimal finite-element cell method - for elastodynamics. *Computer Methods in Applied Mechanics and Engineering*, Vol. 147, pp. 329-355.

Song, Ch.; Wolf, J.P. (2002): Semi-analytical representation of stress singularities as occurring in cracks in anisotropic multi-materials with the scaled boundary finite-element method. *Computers & Structures*, Vol. 80, pp. 83-197.

Suo, Z. (1990): Singularities, interfaces and cracks in dissimilar anisotropic media. *Proceedings of the Royal Society of London*, *Series A*, Vol. 427, pp. 331-358.

Tan, C.L.; Gao, Y.L. (1990): Treatment of bimaterial interface crack problems using the boundary element method. *Engineering Fracture Mechanics*, Vol. 36(6), pp. 919-932.

Tan, C.L.; Gao, Y.L. (1992): Boundary element analysis of plane anisotropic bodies with stress concentrations and cracks. *Composite Structures*, Vol. 20, pp. 17-28.

Tan, C.L.; Wang, X. (2003): The use of quarter-point crack-tip elements for T-stress determination in boundary element method analysis. *Engineering Fracture* Me-

chanics, Vol. 70, pp. 2247-2252.

Wang, X. (2002): Elastic T-stress for cracks in test specimens subjected to non-uniform stresses distributions. *Engineering Fracture Mechanics*, Vol. 69 (12), pp. 1339-1352.

Williams, M.L. (1957): On the stress distribution at the base of a stationary crack. *Journal of Applied Mechanics*, Vol. 24, pp. 109-114.

Williams, M.L. (1959): The stresses around a fault or crack in dissimilar media. *Bulletin of the Seismological Society of America*, Vol. 49, pp. 199-204.

Wolf, J.P.; Song, Ch. (1996): *Finite-Element Modelling of Unbounded Media*. John Wiley & Sons Ltd, Chichester, UK.

Wolf, J.P.; Song, Ch. (2000): The scaled boundary finite-element method - a primer: derivation. *Computers & Structures*, Vol. 78, pp. 191-210.

Yang, S.; Yuan, F.G. (2000): Determination and representation of the stress coefficient terms by path-independent integrals in anisotropic cracked solids. *International Journal of Fracture*, Vol. 101, pp. 291-319.